



## Pectin-based hydrogels and its ferrite nanocomposites for removal of nitro compounds

Faten I. Abou El Fadl<sup>a</sup>, Ghada A. Mahmoud<sup>a,\*</sup>, Nagwa A. Badawy<sup>b</sup>,  
Fatma H. Kamal<sup>b</sup>, Areeg A. Mohamed<sup>b</sup>

<sup>a</sup>National Center for Radiation Research and Technology, Nasr City, Cairo, Egypt, Tel. +2-01065495895; Fax: +2-022 3150336; emails: ghadancrrt@yahoo.com (G.A. Mahomoud), fatenelramly555@yahoo.com (F.I.A. El Fadl)

<sup>b</sup>Faculty of Science, Al Azhar University, Nasr City, Egypt, emails: nagwabadway@yahoo.com (N.A. Badawy), noha\_25\_5@yahoo.com (F.H. Kamal), areeg\_19\_6@yahoo.com (A.A. Mohamed)

Received 29 January 2017; Accepted 7 September 2017

### ABSTRACT

Pectin (acrylic acid-co-acrylamide) (PAA) hydrogel in various formulations was prepared by gamma irradiation and used for preparation of magnetic responsive hydrogels. In situ formation of different metal nanoparticles (Cu and Co) individually and bimetallic clusters inside the hydrogels and magnetic ones were prepared. These prepared nanocomposites were characterized using thermogravimetric analysis, X-ray diffraction analysis and scanning electron microscopy. Transmission electron microscopy confirmed that Co, Cu and magnetic-(Co/Cu) nanoparticles sizes are about 31.25, 50 and 62.5 nm, respectively. The utilization of nanocomposites as a catalyst for the reduction of 2-nitrophenols (2-NP) with very high efficiency was reported. The experimental parameters that affect reduction rates, such as the type of catalyst, NaBH<sub>4</sub> and 2-NP concentration were investigated. The reduction rate constants at different temperatures of 22°C, 36°C and 58°C and activation parameters were calculated. It was found that (PAA)-Cu nanocomposite expressed the greatest reduction ability for 2-NP while (PAA)-Co nanocomposite has low reduction ability.

*Keywords:* Acrylic acid; Pectin; TEM; Nanoparticles; Nitrophenols

### 1. Introduction

Recently, numerous transition metal catalyst systems have been reported for use in hydrolysis reactions. Ni-Ru nanocomposite catalyst, rhodium [1], AlCl<sub>3</sub>, alloys of Ni-Co-B, Ni (0) nanoclusters stabilized with hydrogen phosphate, Co-B/Ni foam, carbon-supported Co-B and Co-P, Co-Ni-P [2], fluorinated cobalt [3], cobalt chloride [4], zirconia [5], and ruthenium are some examples [6–9]. In the utilization of metal nanoparticles as a catalyst, the most important problem is aggregation. Aggregation of nanoparticles causes a reduction in the catalytic activity by decreasing the surface area [10]. Therefore, metallic nanoparticle usage in catalysis, different supporting materials can be

used to prevent agglomeration [11]. It is convenient to use a polymeric network structure for the preparation of metallic particles [12,13]. Hydrogels can provide adaptable support networks with a built in three-dimensional polymeric structure advantageous for in situ metal nanoparticle synthesis [14–16]. The structure containing the hydrophilic groups (–SO<sub>3</sub>H, –OH, –COOH, –NH<sub>2</sub>) allows water and other liquids penetrate inside the hydrogen allowing them to swell and capture metal ions. Because of these functional groups, hydrogels can respond to environmental effects such as pH, ionic strength, temperature, electric and magnetic fields and can even recognize certain molecules. Additionally, hydrogels are biocompatible and have been used as a drug release system control, as sensors in biomedical applications, for separation and purification processes, in tissue engineering, as well as used as a support for catalyst materials [17–19].

\* Corresponding author.

Nitrophenols, one of the derivatives of phenols, are present in high levels in the effluents from numerous industries, including chemical, petrochemical, pharmaceutical, refineries, oil field activities, coal processing, olive oil production, etc. [20]. Phenol is toxic to humans and causes headaches, fainting, vertigo and mental disturbance. Additionally, it can cause several severe ecological and environmental problems in receiving environments. On the other hand, aromatic amines are significant organic pollutants and are intermediate or side products of many industrial products such as dyes, pharmaceuticals, agro-chemicals, cosmetics, photographic chemicals, additives, chelating agents, and so on. For instance, aminophenol is an important reagent in the production of paracetamol, which is used as an analgesic and antipyretic drug [21]. Conventionally, aminophenol is produced by iron-acid reduction of nitrophenol. The major disadvantage of the iron-acid reduction process is the generation of large amounts of Fe-FeO sludge that causes a serious pollution problem. Therefore, a large number of studies for reduction of nitrophenol to aminophenol have been performed over the past few decades. Nowadays, there is a wide choice of techniques available, including activated carbon adsorption, electrochemical, ozonation, biological and chemical procedures, all of which should be economical, environmentally friendly, biodegradable and so on. Sahiner and Sagbas [22] prepared bulk poly(vinylphosphonic acid) p(VPA) hydrogels used as a template for in situ metal nanoparticle preparations of Co, Ni and Cu, by loading the corresponding metal ions from aqueous solution and reduced by  $\text{NaBH}_4$  and the p(VPA)-M (M:Co, Ni, Cu). The hydrogels were used as a soft reactor for the generation of hydrogen by hydrolysis of  $\text{NaBH}_4$  and in the reduction of 4-nitrophenol (4-NP) to 4-aminophenol (4-AP). In the present study, we synthesized a novel co-polymer hydrogel for the first time based on pectin, acrylamide and acrylic acid by the effect of gamma radiation and studied their chemical and physical different properties. Furthermore, its magnetic and magneto-metal nanocomposites were prepared. The advantage of the prepared composite hydrogels is safety and biodegradability, which make them environmentally friendly and also various functionalities, which gave it the high reduction power for nitrophenols. The prepared different nanocomposites were examined as a catalyst for the reduction of 2-nitrophenol to be environmentally friendly 2-aminophenol.

## 2. Materials and methods

### 2.1. Materials

Acrylic acid (AAc; 99%, 72.06 g/mol) was purchased from Sisco research laboratories (Mumbai, India), Acrylamide (AAm; 99%, 71.08 g/mol) was purchased from WINLAB (UK), pectin (Pec; 30,000–100,000 g/mol) was purchased from Oxford laboratory chemicals (Mumbai, India), sodium borohydride ( $\text{NaBH}_4$ ) from Loba Chemie (97%; 37.83 g/mol), 2-NP (98%, 139.11) was purchased from Riedel/de Haen AG Seeize-Hannover, Fe(II)  $\text{FeCl}_2 \cdot 4\text{H}_2\text{O}$  and Fe(III)  $\text{FeCl}_3 \cdot 6\text{H}_2\text{O}$  (99%) were purchased from Acros Organics (Belgium), Cu(II)  $\text{CuSO}_4 \cdot 5\text{H}_2\text{O}$  was purchased from El Nasr Pharmaceutical Chemicals (Egypt),  $\text{CoCl}_2 \cdot 6\text{H}_2\text{O}$  was purchased from Sigma-Aldrich (USA).

### 2.2. Radiation preparation of hydrogel

Firstly, 5% (wt/v) concentration of AAm, Pec and AAc were prepared by dissolving the specified masses in distilled water; different compositions of (PAA) hydrogel were prepared as shown in Table 1. Then the mixtures were mixed by a magnetic stirrer for 2 h to form homogenous solutions. Finally, the solutions were filled into test tubes (inner diameter 5 mm) and subjected to 40 KGy of gamma radiation at a dose rate of 3.52 kGy/h. The prepared hydrogels were extracted in distilled water at  $80^\circ\text{C}$ – $100^\circ\text{C}$  for 2 h, in order to remove the non-cross-linked polymer, and then the hydrogels were dried at  $50^\circ\text{C}$  in the oven.

### 2.3. Preparation of magnetic hydrogels

The magnetic particle preparation procedure was carried out by absorption technique. Briefly, a cleaned and known amount of dried hydrogel (PAA) of different compositions were placed in  $0.5 \text{ mol dm}^{-3}$  Fe(II) and Fe(III) ions aqueous solution, where Fe(II):Fe(III) mole ratio was 1:2 for 12 h. Then they underwent a washing period in which iron ion-loaded hydrogels were kept in distilled water for 24 h to remove unbound and/or physically bound metal ions. After washing, iron ion (Fe(II) and Fe(III))-loaded hydrogels were transferred into  $0.5 \text{ mol dm}^{-3}$  of sodium hydroxide solution and the reaction proceeded for 5 h in a water shaker bath at an ambient temperatures. Finally, the obtained magnetic hydrogels were cleaned by washing with deionized water for another 12 h and dried in oven at  $40^\circ\text{C}$ .

### 2.4. Loading of metal ions into hydrogels

To load the (PAA) hydrogel and magnetic hydrogel with metal ions, 0.1 g of dried hydrogel was placed into 50 mL of 250, 500 and  $1,000 \text{ mg dm}^{-3}$  metal ion solution to load hydrogel with Co(II) or Cu(II). Absorption procedure was performed by a magnetic stirrer setup at room temperature for 24 h. At the end of the metal ion absorption period, the loaded hydrogels were kept in distilled water for another 24 h to remove unbound metal ions. For the preparation of bimetallic cluster nanoparticles, 0.1 g of dried hydrogel was placed into a mixture of  $250 \text{ mg dm}^{-3}$  Co(II) and  $250 \text{ mg dm}^{-3}$  Cu(II) solution at ratios (1:1, 1:2 and 2:1 Co:Cu) in the same way as mentioned above. The absorbed amounts of Co(II) and Cu(II) were determined from the metal ion solutions using ICP-AES (inductive coupled plasma-atomic spectrometry (Varian Liberty II AX Sequential). Again, after metal ion loading, the hydrogels were transferred to deionized water for cleaning for another 24 h.

Table 1  
The different feed mixture compositions of (PAA) hydrogel

Symbol	AAc, %	AAm, %	Pec, %	G, %	S, %
PAA <sub>1</sub>	3	1	1	97.4	91.2
PAA <sub>2</sub>	2	1.5	1.5	95.9	98.9
PAA <sub>3</sub>	1	2	2	89.6	118.1
PAA <sub>4</sub>	1	1.5	2.5	84.8	110
PAA <sub>5</sub>	0.5	1.5	3	75.1	200

G% is the gel percentage; S% is the swelling percentage after 24 h.

### 2.5. In situ preparation of metallic nanocomposites

The metal ions inside the hydrogels were reduced by transferring these metal ions loaded magnetic and non-magnetic hydrogels into 25 mL of 1 mg dm<sup>-3</sup> NaOH for 3 h then in 20 mL of 0.5 mg dm<sup>-3</sup> NaBH<sub>4</sub> for another 20 h. Soaking them in deionized water for 12 h and drying in the oven at 40°C. The formed black-colored hydrogel-metal nanoparticle composites were cut into smaller pieces and used as a catalyst throughout this 2.6.

### 2.6. Catalytic reduction studies of 2-NP

Reaction conditions used for reduction of 2-NP were as follows: 10 mL of 0.01 mg dm<sup>-3</sup> of 2-NP was mixed with 10 mL of 0.4 mg dm<sup>-3</sup> NaBH<sub>4</sub> then 0.08 g of magnetic and non-magnetic (PAA) metal nanocomposites was added to the solution mixture to initiate the reduction of 2-NP to its 2-AP. During the reduction procedure, specific volumes of samples were taken from the reduction medium at specific time intervals to observe the conversion of 2-NP to 2-AP by using UV-Vis spectrophotometer at 400 nm. The effect of NaBH<sub>4</sub> concentration on the reduction rate of 2-NP to 2-AP is also recorded. To investigate the effect of temperature, the reduction reaction was carried out at three different temperatures (22°C, 36°C, and 58°C).

### 2.7. Characterization

Thermogravimetric analysis (TGA) studies were carried out on a Shimadzu (Japan) 30 (TGA-30) at a heating rate of 10°C/min in the air over a temperature range from room temperature to 600°C. The primary TGA thermograms were used to determine the different kinetic parameters and to study the order of thermal decomposition reaction.

The surface morphology of different hydrogel composition samples, magnetic and non-magnetic nanocomposites were detected using scanning electron microscopy (SEM; JSM-5400, JEOL, Japan). A sputter coater was used to pre-coat conductive gold on the fracture surface before observing the microstructure at 10 kV. Energy dispersive X-ray (EDX) analysis was carried out during the surface analysis done by SEM (JSM-5400, JEOL, Japan).

The X-ray diffraction (XRD) analysis was performed using XD-DI Series (Shimadzu, Japan) apparatus using nickel-filtered and Cu-K target.

Transmission electron microscopy (TEM) measurements were performed using TEM JEOL (JEM-100cx; Japan). The powders of prepared nanocomposites were suspended in water and a drop of the resultant mixture was deposited on an ultra-thin carbon supported Cu grid and air-dried.

A UV/VIS spectrometer model UV-Analytic Jena AG (Specord 210, German) was used at a wavelength of 400–1,100 nm and throughout this work.

## 3. Results and discussions

### 3.1. Preparation mixture compositions of PAA hydrogel

Pectin in this work is used to prepare biodegradable hydrogel with acrylamide and acrylic acid by the effect of gamma radiation. PAA is a copolymer composed of natural polymer (pectin) to impart biodegradability to the system and polyacrylic acid and polyacrylamide to provide the good

mechanical properties to the prepared system beside the various functionality, safety and cheap. Table 1 represents the ratios of polymers used to prepare different compositions of the PAA hydrogel and the calculated gel percentage and swelling percentage. From Table 1, it can be obtained that the prepared hydrogel of formula PAA<sub>2</sub> has the most suitable of both gel and swelling percent for the application. Hence, the preparation of PAA<sub>2</sub> is examined for loading of magnetic and metal nanoparticles and chosen for characterization.

### 3.2. Characterization of hydrogel

#### 3.2.1. Thermogravimetric analysis

The amounts of Co and Cu metal nanoparticles in the magnetic and non-magnetic PAA<sub>2</sub> hydrogels were determined with TGA measurements by comparing empty PAA<sub>2</sub> hydrogel with metal nanoparticle containing magnetic and non-magnetic hydrogel composites. It is observed from the corresponding thermograms of all different hydrogel nanocomposites in Fig. 1 that all nanocomposites hydrogels undergo similar patterns with sharp weight loss at about 450°C–500°C. In addition, the amounts of metal nanoparticles (which indicated by the weight loss percentage) in the prepared hydrogels were recorded and summarized in Table 2,

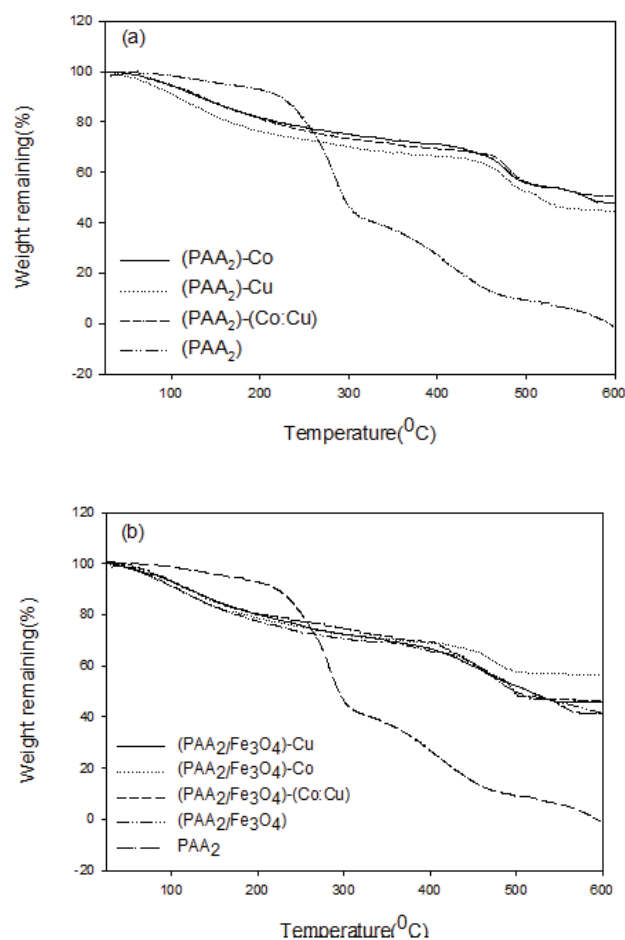


Fig. 1. TGA thermograms of (a) (PAA<sub>2</sub>)-metallic nanocomposites and (b) (PAA<sub>2</sub>)-magneto metallic nanocomposites.

where the TGA results revealed that PAA<sub>2</sub> hydrogels give 56.41, 50.57, 47.79, 46.42, 45.69, 44.83, 41.54, 1.46 wt% for (PAA<sub>2</sub>/Fe<sub>3</sub>O<sub>4</sub>)-Co, (PAA<sub>2</sub>)-(Co:Cu), (PAA<sub>2</sub>)-Co, (PAA<sub>2</sub>/Fe<sub>3</sub>O<sub>4</sub>)-(Co:Cu), (PAA<sub>2</sub>/Fe<sub>3</sub>O<sub>4</sub>)-Cu, (PAA<sub>2</sub>)-Cu, (PAA<sub>2</sub>/Fe<sub>2</sub>O<sub>3</sub>) and PAA<sub>2</sub> hydrogel, respectively. This indicates that the (PAA<sub>2</sub>)

hydrogel having the highest Co and Fe nanoparticles that gives the highest weight residue (56.41) as shown in Table 2 than other hydrogel nanocomposites also having the highest thermal stability.

### 3.2.2. Scanning electron microscopy

SEM is another helpful technique for studying the change in morphological structure of (PAA<sub>2</sub>) hydrogel nanocomposites containing Cu, Co, bimetallic (Co:Cu) (1:1), magnetic (Co:Cu) (1:1) nanoparticles compared with unloaded (PAA<sub>2</sub>) hydrogel as shown in Figs. 2(a)–(e). Obviously, as it appears in Fig. 2(a) that represents the surface morphology of PAA before loading with metal nanoparticles, the surface appeared smooth with very few cracks and hills on it, while in Figs. 2(b) and (c) that represent the surface morphology of (PAA<sub>2</sub>)-Co and (PAA<sub>2</sub>)-Cu, the surface appeared rough and porous due to the presence of different metals beside each other. Fig. 2(d) represents the surface morphology of (PAA<sub>2</sub>)-(Co:Cu) which

Table 2

The percentage weight residues of free, metal loaded and magneto-metal loaded (PAA) nanocomposites

Symbol	Weight residue, %	Symbol	Weight residue, %
(PAA <sub>2</sub> )-Cu	44.83	(PAA <sub>2</sub> /Fe <sub>3</sub> O <sub>4</sub> )-Cu	45.69
(PAA <sub>2</sub> )-Co	47.79	(PAA <sub>2</sub> /Fe <sub>3</sub> O <sub>4</sub> )-Co	56.41
PAA <sub>2</sub> -(Co:Cu)	50.57	(PAA <sub>2</sub> /Fe <sub>3</sub> O <sub>4</sub> )-(Co:Cu)	46.42
PAA <sub>2</sub>	1.46	(PAA <sub>2</sub> /Fe <sub>3</sub> O <sub>4</sub> )	41.54

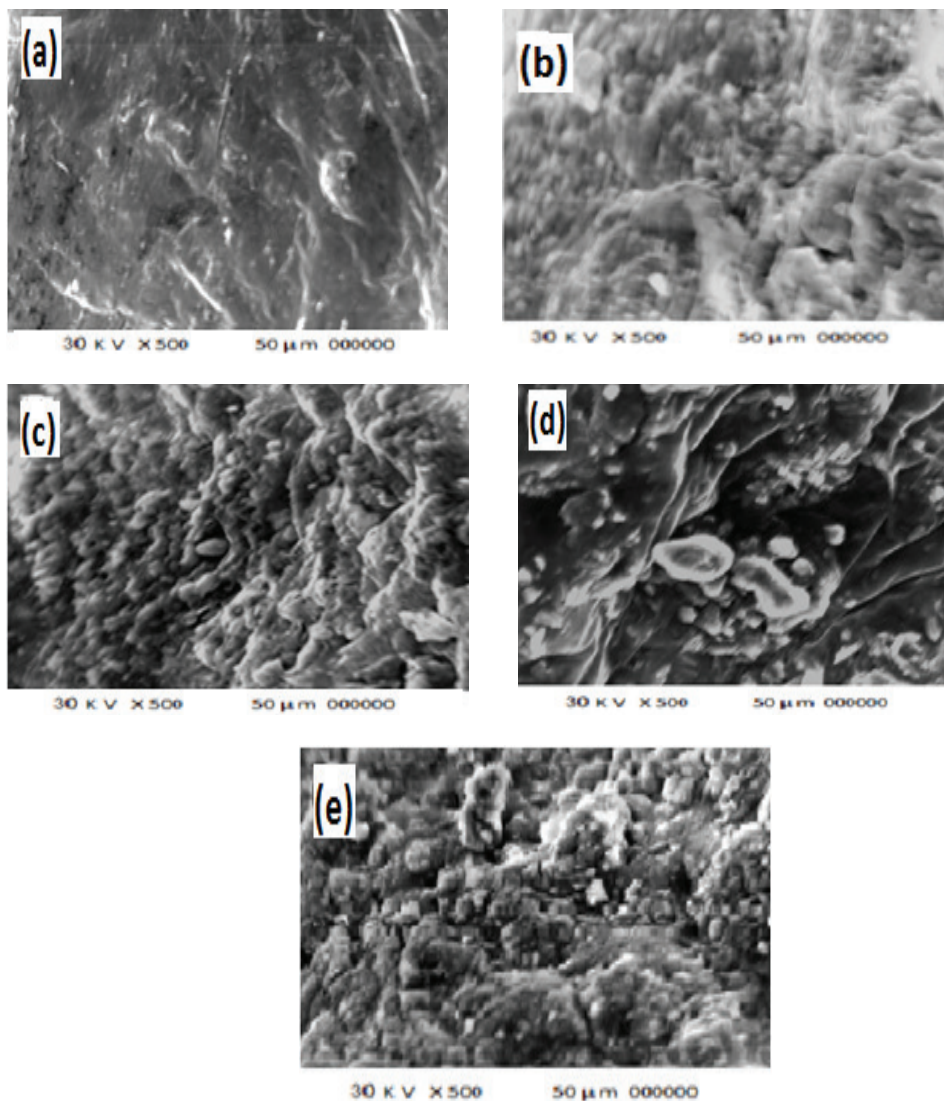


Fig. 2. SEM images of (a) (PAA<sub>2</sub>) unloaded hydrogel, (b) (PAA<sub>2</sub>)-Co, (c) (PAA<sub>2</sub>)-Cu, (d) (PAA<sub>2</sub>)-(Co:Cu)(1:1) and (e) (PAA<sub>2</sub>/Fe<sub>3</sub>O<sub>4</sub>)-(Co:Cu)(1:1) nanocomposites.

observed rough and porous surface with aggregation in some places. While in Fig. 2(e), the surface of  $(PAA_2/Fe_3O_4)-(Co:Cu)$  nanocomposites are observed as a compact and very rough surface greater than when compared with the  $(PAA_2)-Co$ ,  $(PAA_2)-Cu$  and  $(PAA_2)-(Co:Cu)$  due to the presence of Fe nanoparticles that increases the intensity of nanoparticles and also causes aggregation to some extent between the formed nanoparticles in the hydrogels.

### 3.2.3. Transmission electron microscopy

TEM is used mainly to confirm the preparation of metal particles in the nanoscale and also it is very useful in predicting the size of the formed metal nanoparticles. Figs. 3(a)–(c) illustrate the TEM images of  $(PAA_2)-Co$ ,

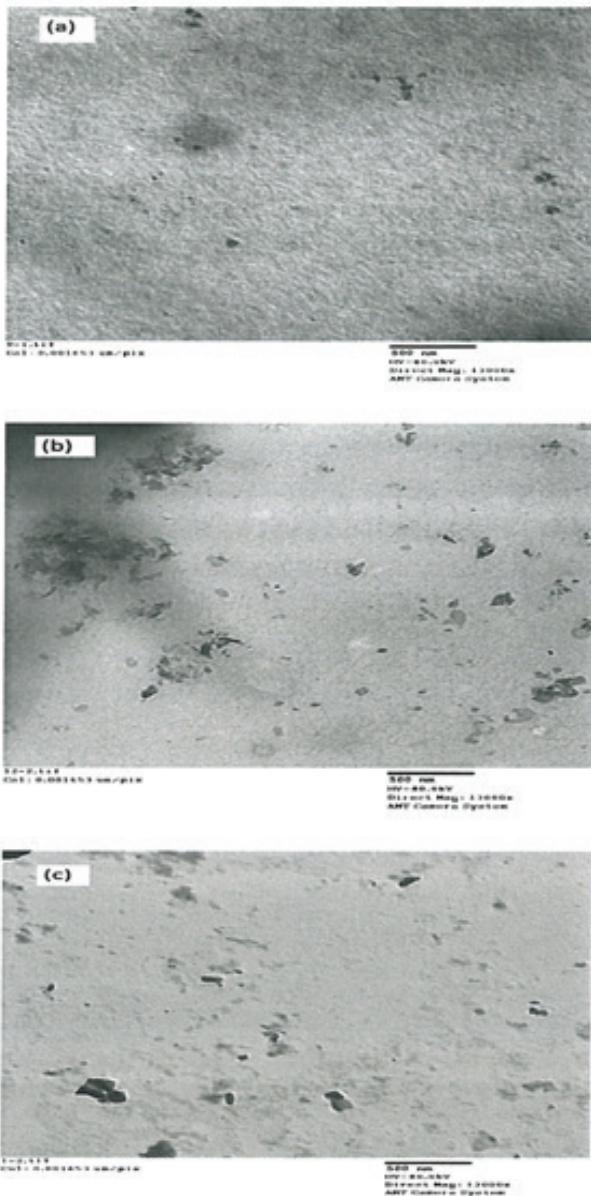


Fig. 3. TEM images of (a)  $(PAA_2)-Co$ , (b)  $(PAA_2/Fe_3O_4)-(Co:Cu)$  (1:1) and (c)  $(PAA_2)-Cu$  nanocomposites.

$(PAA_2)-Cu$ , and  $(PAA_2/Fe_3O_4)-(Co:Cu)$  (1:1) nanocomposites. As revealed by TEM images, the obtained Co, Cu and magnetic-(Co:Cu) nanoparticles sizes were approximately 31.25, 50 and 62.5 nm, respectively. It is also clear from the images, the presence of agglomeration in some places of the samples in agreement with the SEM micrographs.

### 3.2.4. Energy dispersive X-ray spectroscopy

The presence of metal nanoparticles and iron species inside  $(PAA_2)$  nanocomposite is confirmed by EDX. Fig. 4 shows EDX analysis for  $(PAA_2)-Co$ ,  $(PAA_2)-Cu$ , and  $(PAA_2/Fe_3O_4)-(Co:Cu)$  (1:1) nanocomposites. It can be obtained that  $(PAA_2/Fe_3O_4)-Co$  nanocomposite gives 28.48% of Fe and 71.52% of Co  $(PAA_2/Fe_3O_4)-Cu$  nanocomposite gives 14.22% of Fe and 85.78% of Cu and  $(PAA_2/Fe_3O_4)-(Co:Cu)$  (1:1) nanocomposite gives 6.53% of Fe, 49.52% of Co and 43.95% of Cu.

### 3.2.5. X-ray diffraction

XRD analysis of Co, Cu and magnetic-based nanoparticles supported on  $(PAA)$  hydrogel is shown in Figs. 5(a) and (b). The figures illustrate the XRD patterns of the  $(PAA_2)$ ,  $(PAA_2)-Co$ ,  $(PAA_2)-Cu$  and  $(PAA_2)-Co-Cu$ , and their magnetic counterparts  $(PAA_2/Fe_3O_4)-Co$ ,  $(PAA_2/Fe_3O_4)-Cu$ , and  $(PAA_2/Fe_3O_4)-(Co:Cu)$  (1:1) nanocomposites. It can be observed in Fig. 5(a) that  $PAA_2$  hydrogel has some crystallinity due to the strong interaction between polymeric chains through intermolecular hydrogen bonding between its hydroxyl groups. For  $(PAA_2)-Co$ , the characterized peaks of Co(0) nanoparticles are observed, which are at  $2\theta = 42^\circ$ ,  $47^\circ$  and  $76^\circ$ , which

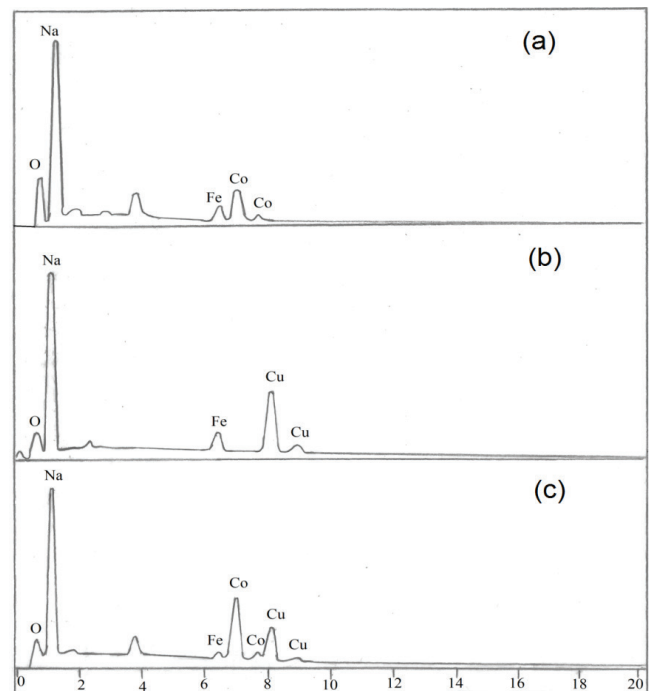


Fig. 4. EDX micrographs of (a)  $(PAA_2/Fe_3O_4)-Co$ , (b)  $(PAA_2/Fe_3O_4)-Cu$  and (c)  $(PAA_2/Fe_3O_4)-(Co:Cu)$  (1:1) nanocomposites.

correspond to the 100, 101 and 110 planes of a face-centered cubic structure. Typical XRD patterns were reported throughout the literature of Cu(0) [23]. For (PAA)<sub>2</sub>-Co, the characterized peaks of Cu(0) nanoparticles are observed by peaks at  $2\theta = 43.3^\circ$ ,  $50.4^\circ$  and  $73.4^\circ$ , which correspond to the 111, 200 and 220 planes of a face-centered cubic structure [24]. The XRD shows beside metallic Cu and Co peaks, in the range  $2\theta$  of 10 to  $2\theta = 30$ , may belong to monoclinic Co and Cu oxides that may be formed during the reaction [25]. The presence of Co and Cu oxides is attributed to the incomplete reduction of the divalent metal ions or to re-oxidation of metallic Co and Cu. The XRD patterns for the magnetic nanocomposites (Fig. 5(b)), moreover, the peaks mentioned above the characterized peaks of Fe(0) nanoparticles are observed at  $2\theta = 45^\circ$ ,  $65^\circ$  and  $83^\circ$ , which correspond to the 110, 200 and 211 planes of a face-centered cubic structure.

### 3.2.6. Magnetic properties of (PAA/Fe<sub>3</sub>O<sub>4</sub>) and (PAA/Fe<sub>3</sub>O<sub>4</sub>)-metal nanoparticles

The magnetic properties of polymer hydrogels are determined by embedding magnetic particles. Among these particles, metal oxides are often preferred over pure metals (Fe, Co and Ni) [26] because they are more stable to oxidation. The magnetic properties of metal oxides depend upon their chemical composition, their size, shape, their crystal structure, the degree of crystallinity, etc. The magnetization curves of the PAA<sub>2</sub>/Fe<sub>3</sub>O<sub>4</sub> and PAA<sub>2</sub>/Fe<sub>3</sub>O<sub>4</sub>-bimetallic

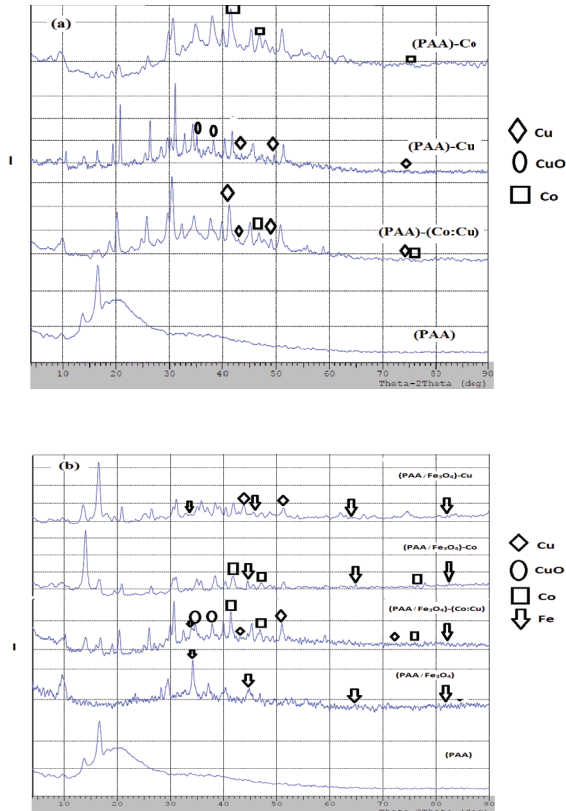


Fig. 5. XRD patterns of (a) (PAA) and (PAA)-M, (b) (PAA), (PAA/Fe<sub>3</sub>O<sub>4</sub>) and (PAA/Fe<sub>3</sub>O<sub>4</sub>)-M (M:Co, Cu, (Co:Cu)(1:1)) nanocomposites.

nanocomposite are shown in Fig. 6. The M-H curve was obtained in the presence of a magnetic field of 17.5 kOe at room temperature. It is observed that the PAA<sub>2</sub>/Fe<sub>3</sub>O<sub>4</sub> and PAA<sub>2</sub>/Fe<sub>3</sub>O<sub>4</sub>-metal nanoparticles exhibit both coercivity (H<sub>c</sub>) and remnant magnetization (M<sub>r</sub>), which proves that both PAA<sub>2</sub>/Fe<sub>3</sub>O<sub>4</sub> and PAA<sub>2</sub>/Fe<sub>3</sub>O<sub>4</sub>-metal nanoparticles are superparamagnetic in nature. Moreover, the M-H curve does not saturate up to the maximum applied field. The reason for the superparamagnetic nature of the NPs is essentially due to the very small size. The smaller size may be considered as an equivalent to an individual magnetic domain where the energy barrier for its spin reversal easily overcomes by thermal vibrations resulting in superparamagnetic nature of nanosize particles. Nishio et al. [27] reported that Fe<sub>3</sub>O<sub>4</sub> NPs having a particle size nearly 50 nm or even less may be considered as a single.

### 3.3. Sorption of metal ions in PAA hydrogel

The amount of metal loaded on PAA and PAA/Fe<sub>3</sub>O<sub>4</sub> hydrogel was determined and shown in Figs. 7(a) and (b). The absorption experiment was carried out by using three concentrations 250, 500, and 1,000 mol dm<sup>-3</sup> of metal ions solutions. It is noticed that the amounts of Co ions absorbed by hydrogel were 23.9, 87.9, 80.59 mg/g at feed solution concentration of 250, 500, 1,000 mol dm<sup>-3</sup>, respectively. On the other hand, the amount of Cu ions absorbed were 113.56, 82.4, 121.6 mg/g at initial feed solution concentrations 250, 500, 1,000 mg dm<sup>-3</sup>, respectively. It is observed that the amount of Co ions which absorbed by dry magnetic hydrogel (Fig. 7(b)) were 24.8, 48.08 and 65.96 mg/g of hydrogels, and the amount of absorption of Cu ions were 92.59, 63.47 and 64.65 mg/g of hydrogels at initial metal solution concentrations of 250, 500, 1,000 mol dm<sup>-3</sup>, respectively. Finally, Fig. 8 shows the amount of (Co:Cu) bimetallic ions at different ratios [(1:1), (1:2) and (2:1)] which absorbed from metal ion solution concentration of 250 mol dm<sup>-3</sup>. It is found that the amounts absorbed by the PAA hydrogel were 12.55, 22.3, and 23.01 mg dm<sup>-3</sup>, respectively, and the amounts absorbed by PAA/Fe<sub>3</sub>O<sub>4</sub> nanocomposite were 13.37, 9.42 and 6.32 mg/g, respectively. After absorption of the different metal ions and

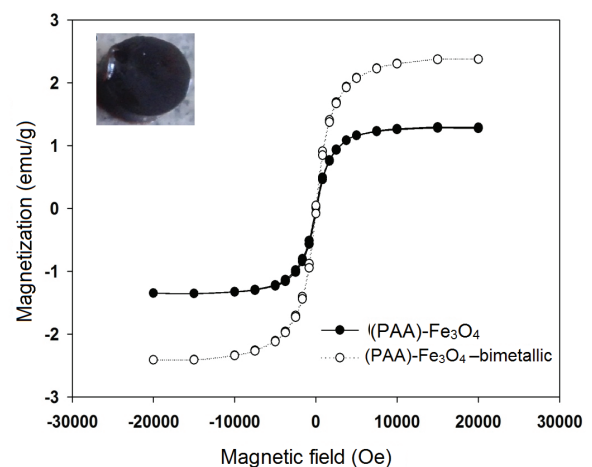


Fig. 6. M-H curve of (PAA)-Fe<sub>3</sub>O<sub>4</sub> and (PAA)-Fe<sub>3</sub>O<sub>4</sub>-bimetallic nanocomposites.

bimetal ions on the specified hydrogels, the reduction of the metal ions to its counterpart metal nanoparticles was carried out by using  $\text{NaBH}_4$  as a reducing agent at a concentration of  $0.5 \text{ mol dm}^{-3}$ .

3.4. Catalytic reduction of 2-NP

In this study, the prepared Co, Cu, magnetic-Co, magnetic-Cu, metal nanoparticles inside environmentally friendly PAA hydrogels were examined for the reduction of 2-NP in the presence of aqueous  $\text{NaBH}_4$ . 2-NP has maximum absorption at 412 nm, in the reaction mixture and the decrease in these absorption bands was tracked by UV-Vis spectrophotometers, the evidence of the complete reduction

of 2-NP is the new band formed at 290 nm corresponding to the formation of 2-AP. In this respect different parameters that affect the reduction process, such as the effect of different compositions of hydrogel, effect of different metal type on reduction and the time taken to finish the reduction of 2-NP to 2-AP,  $\text{NaBH}_4$  concentration, temperature and concentration of 2-NP are briefly studied and evaluated later. To examine the catalytic reduction activity of Co and Cu impeded into non-magnetic and magnetic PAA of different compositions for the reduction 2-NP were used. The reduction of 2-NP was occurring with the addition of 0.08 g of PAA nanocomposites catalyst system through the reaction medium which composed of  $0.01 \text{ mol dm}^{-3}$  2-NP and  $0.4 \text{ mol dm}^{-3}$   $\text{NaBH}_4$  at  $22^\circ\text{C}$  and measured by UV spectra.

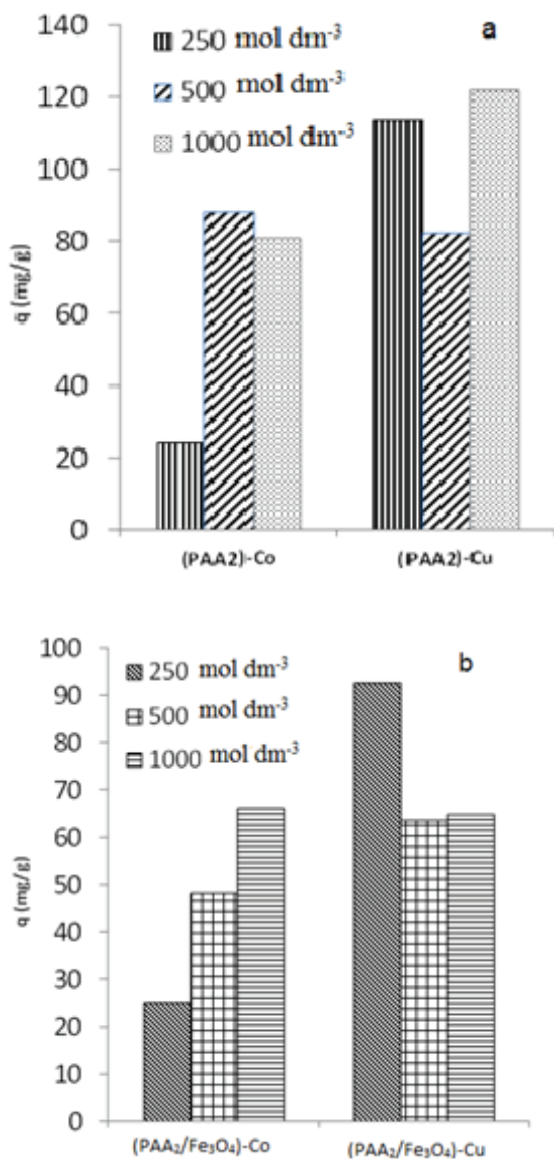


Fig. 7. The amount of metal ions loaded in (PAA<sub>2</sub>) hydrogel at different concentrations of metal ions solution (a); the amount of metal ions loaded in (PAA<sub>2</sub>/Fe<sub>3</sub>O<sub>4</sub>) hydrogel at different concentrations of metal ions solution (b).

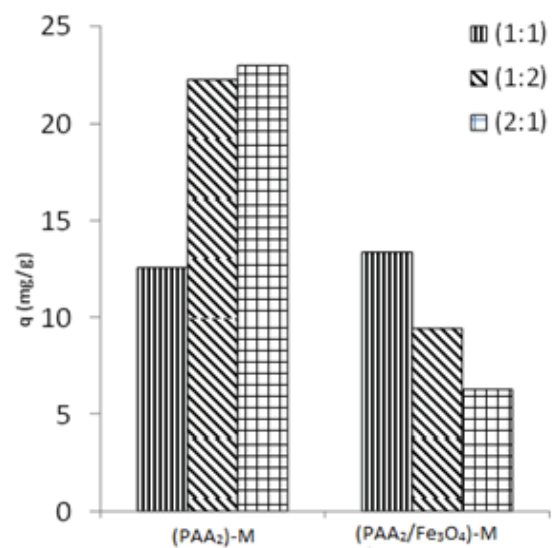


Fig. 8. The amount of bimetallic ions loaded in (PAA<sub>2</sub>) and (PAA<sub>2</sub>/Fe<sub>3</sub>O<sub>4</sub>) hydrogels at different ratios of bimetallic ions (M:(Co:Cu)).

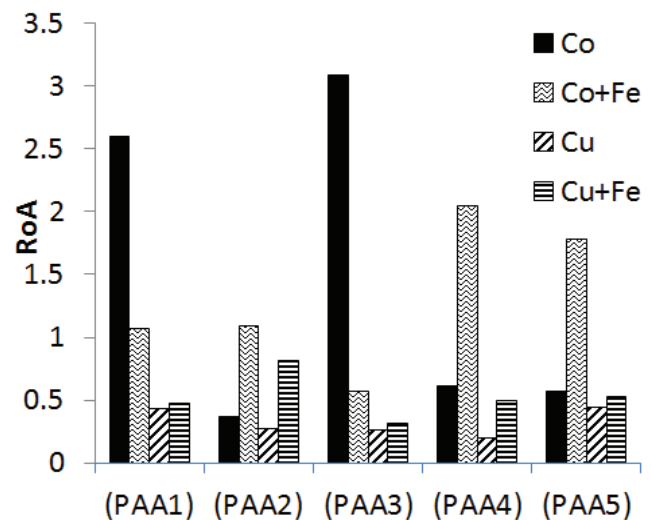


Fig. 9. The effect of different compositions of (PAA) hydrogel on the reduction of 2-NP.

As we can be seen from Fig. 9, PAA<sub>2</sub> nanocomposites loaded with different metals has almost higher reduction ability for 2-NP than the other compositions because it was given after the reduction of 2-NP the lowest remaining of absorption peak for non-reduced 2-NP (remaining of absorption RoA). Depending on the above results, the PAA<sub>2</sub>-nanocomposite is selected to be used as a catalyst for the reduction of 2-NP in the next steps. It can be observed that the catalytic activity depends on the type of the trapped metal; the nanocomposite-trapped Cu metal has a higher catalytic power than that trapped Co metal. The two heavy metals Co and Cu have different shape, size, and activity so this will as a result affect on their catalytic power. Furthermore, the magnetic nanocomposite has higher catalytic activity than non-magnetic one due to the dual effect of metal, Cu or Co, and Fe<sub>3</sub>O<sub>4</sub>. This is due to Fe<sub>3</sub>O<sub>4</sub> is not only a support to prevent aggregation of Cu NPs, but also can provide a synergistic effect, which allow more molecules to be in contact with the surface of Cu NPs. The Cu/Fe<sub>3</sub>O<sub>4</sub> nanocomposite has a higher surface area which can provide more active sites for adsorption of reactants via

stacking  $\pi$ - $\pi$  interactions. Such adsorption provides a relatively high concentration of reactant molecules that are closer to the Cu NPs on Fe<sub>3</sub>O<sub>4</sub>, leading to highly efficient contact between them.

#### 3.4.1. Effect of different concentrations of NaBH<sub>4</sub>

Different concentrations of NaBH<sub>4</sub> 0.2, 0.4 and 0.6 mol dm<sup>-3</sup> were used for the reduction of 2-NP to 2-AP, and the results are shown in Fig. 10. It is noticed that the reduction rate of 2-NP by using (PAA<sub>2</sub>)-Cu as a catalyst (Fig. 10(a)) was increased with increasing the NaBH<sub>4</sub> concentration. On the other hand, by using (PAA<sub>2</sub>/Fe<sub>3</sub>O<sub>4</sub>)-Cu as a catalyst, it is found that the reduction rate was decreased with increasing the NaBH<sub>4</sub> concentration as in Fig. 10(b). While using (PAA<sub>2</sub>/Fe<sub>3</sub>O<sub>4</sub>)-Co nanocomposite caused the highest reduction rate at 0.4 mol dm<sup>-3</sup> of NaBH<sub>4</sub> as shown in Fig. 10(c). The change in the reduction rate constant with changing the NaBH<sub>4</sub> concentration for different PAA<sub>2</sub> nanocomposites is shown in Fig. 10(d).

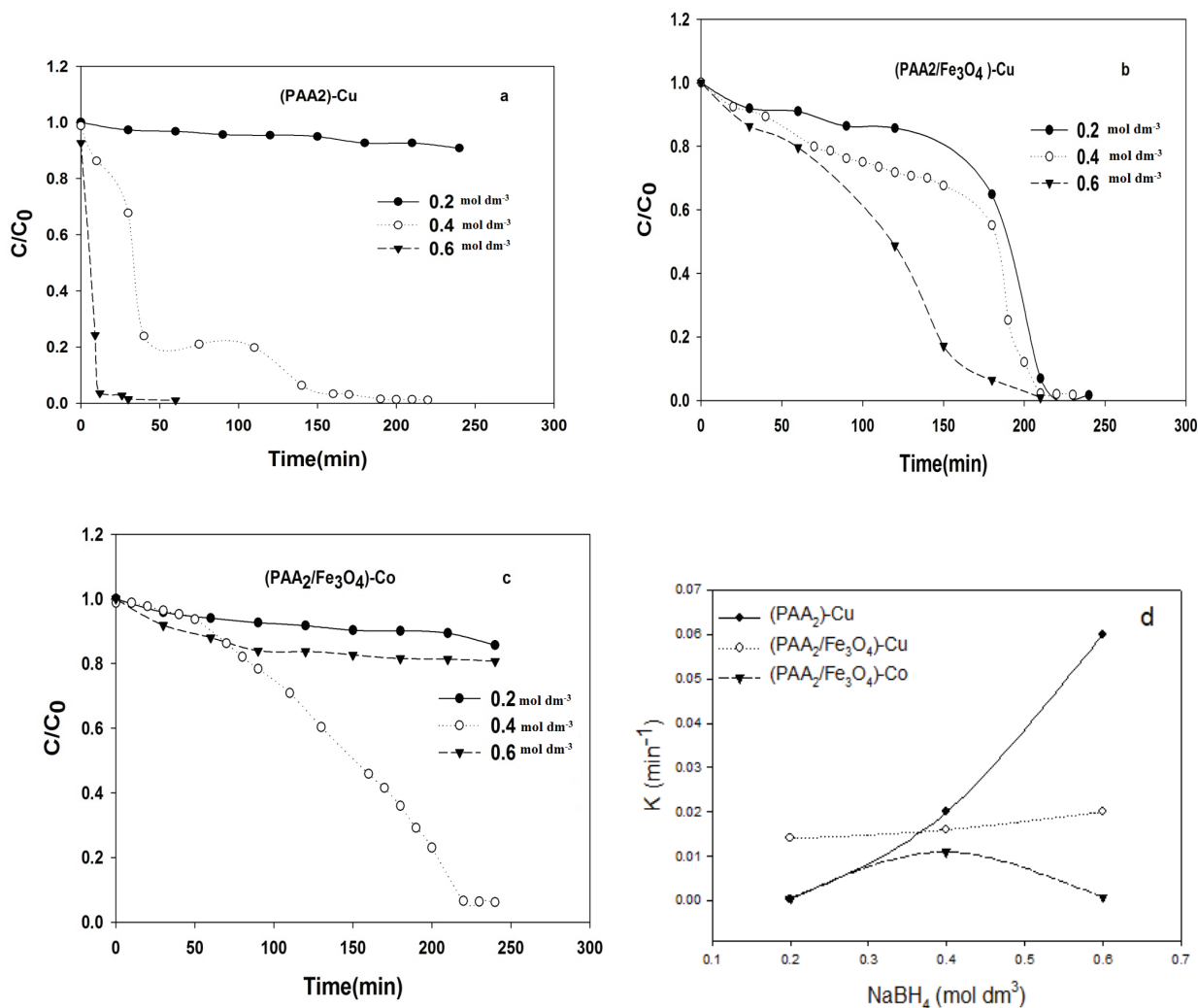


Fig. 10. The effect of different NaBH<sub>4</sub> concentrations on the reduction reaction of 2-NP by different (PAA<sub>2</sub>)-M nanoparticles (Reaction condition: 10 mL [2-NP] = 0.01 mg dm<sup>-3</sup> and 0.08 g catalyst, 22°C) (a, b, c), the change in the reduction rate constant with changing the NaBH<sub>4</sub> concentration for different (PAA<sub>2</sub>) nanocomposites (d).

3.4.2. Effect of different concentrations of 2-NP

It is important to study the effect of 2-NP concentration on its reduction so in this respect, different concentrations of 2-NP 0.005, 0.01 and 0.015 mol dm<sup>-3</sup> were used. Fig. 11 shows the reduction of different concentrations of 2-NP using of PAA<sub>2</sub>-Cu nanocomposite as a catalyst. It is noticed that, as the 2-NP concentration increases the reduction rate decreases, this is plausible as the concentration decrease, the amount of catalyst per unit of 2-NP increased relatively. This trend was also observed by other authors [28]. A high concentration of 2-NP molecules leads to nearly full coverage of the surface of the nanoparticles with 2-NP. Competitive absorption of the reactants thus results in slowing down the reaction.

3.4.3. Effect of different temperature

To determine the effect of temperature on the reduction of 2-NP to be 2-AP catalyzed by (PAA<sub>2</sub>)-Cu and (PAA<sub>2</sub>/Fe<sub>3</sub>O<sub>4</sub>)-M, the reaction was carried out at different temperatures (22°C, 36°C and 58°C) using 0.4 mol dm<sup>-3</sup> NaBH<sub>4</sub> and 0.01 mol dm<sup>-3</sup> 2-NP are shown in Fig. 12 where it is found that the reduction rate constant is increased with increasing temperature when (PAA<sub>2</sub>)-Cu and (PAA<sub>2</sub>/Fe<sub>3</sub>O<sub>4</sub>)-Cu nanocomposites are used as a catalyst system shown in Figs. 12(a) and (b), respectively. However, when using (PAA<sub>2</sub>/Fe<sub>3</sub>O<sub>4</sub>)-Co as a catalyst system, there is no reduction ability occurred by raising the temperature as Fig. 12(c). The value of the rate constants of different (PAA) nanocomposites at different temperatures was calculated and summarized in Table 3. The activation parameters for both reduction reactions with the synthesized (PAA<sub>2</sub>)-M catalyst systems were calculated using the well-known Arrhenius Eq. (1) and Eyring equations Eq. (2) as shown:

$$\ln k = \ln A - \frac{\Delta E_a}{RT} \tag{1}$$

$$\ln \frac{k}{T} = \ln \left( \frac{k_B}{h} \right) - \frac{\Delta H}{R} \left( \frac{1}{T} \right) \tag{2}$$

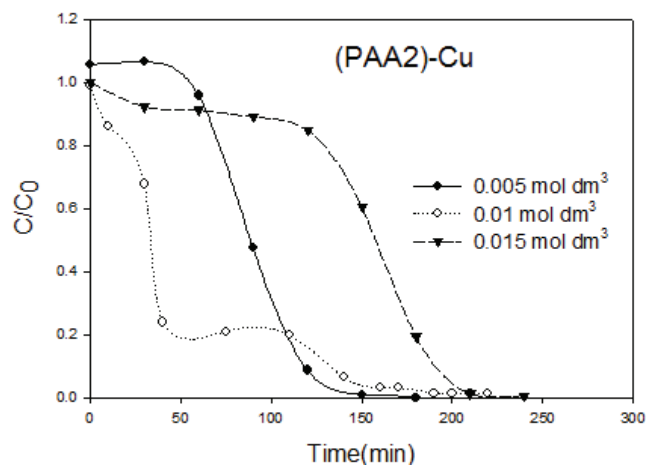


Fig. 11. The effect of 2-NP concentration on the reduction rate using (PAA<sub>2</sub>)-Cu as a catalyst.

where  $E_a$  is the activation energy,  $T$  is absolute temperature;  $k_B$  is the Boltzmann constant  $1.381 \times 10^{-23} \text{ JK}^{-1}$ ,  $h$  is the Planck constant ( $0.626 \times 10^{-34} \text{ J s}$ ,  $\Delta H$  is the activation enthalpy,  $\Delta S$  is the activation entropy and  $R$  is the ideal gas constant  $8.314 \text{ JK}^{-1} \text{ mol}^{-1}$ . The different values of  $E_a$ ,  $\Delta S$ ,  $\Delta H$ ,  $K$  the reduction rate constant, and  $k$  the activity factor for different PAA<sub>2</sub> nanoparticles at various temperatures are

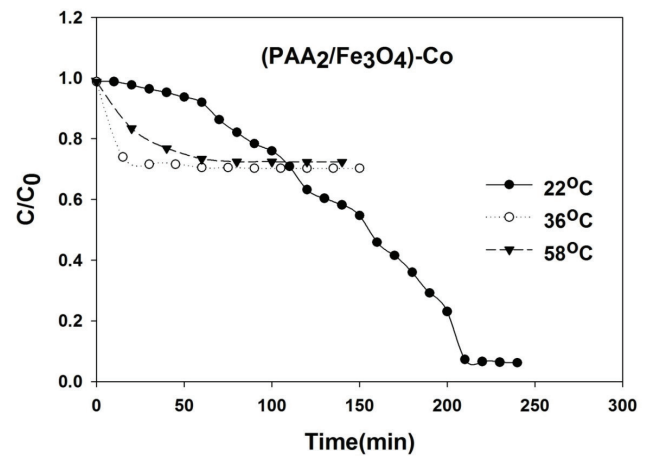
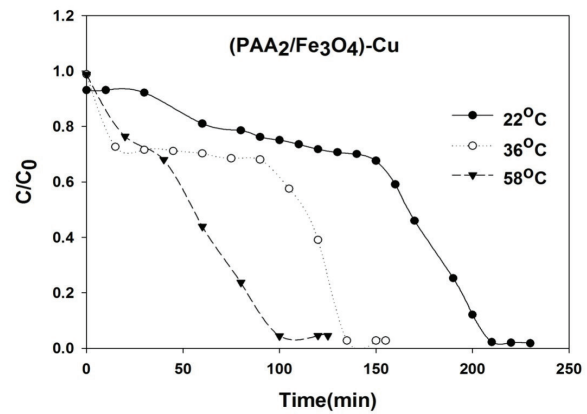
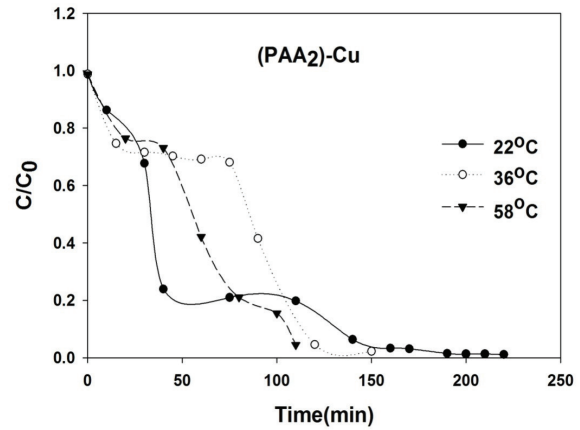


Fig. 12. The effect of temperature on the reduction reaction of (0.01 mg dm<sup>-3</sup>) 2-NP by different (PAA<sub>2</sub>)-metallic nanoparticles in the presence of aqueous (0.4 mg dm<sup>-3</sup>) NaBH<sub>4</sub>.

Table 3

The change in the reduction rate constants of 2-NP at different temperatures and activation parameters for different (PAA<sub>2</sub>) nanocomposites

Composition	Temperature (°C)	<i>k</i> (min <sup>-1</sup> )	<i>K</i> (S <sup>-1</sup> g <sup>-1</sup> )	<i>E<sub>a</sub></i> (kJ mol <sup>-1</sup> )	$\Delta H$ (kJ mol <sup>-1</sup> )	$\Delta S$ (J mol <sup>-1</sup> k <sup>-1</sup> )
(PAA <sub>2</sub> )-Cu	22	0.021	0.26	12.18	9.477	-244.59
	36	0.027	0.34			
	58	0.036	0.45			
(PAA <sub>2</sub> /Fe <sub>3</sub> O <sub>4</sub> )-Cu	22	0.015	0.19	13.32	10.77	-243.34
	36	0.016	0.2			
	58	0.028	0.35			

calculated and listed in Table 3. It is noticed from the data of activity factors at various temperatures in Table 3, the activity factor increased with increasing temperature and also the activity factor of (PAA<sub>2</sub>/Fe<sub>3</sub>O<sub>4</sub>)-Cu as an example, is higher than that for PAA<sub>2</sub> in agreement with the activation parameters obtained for this system. In addition, the activity factor of the prepared nanocomposite hydrogels were calculated to compare the results obtained for this work with others reported in the literature, it has been getting a satisfactory result [29–31]. It is also noticed that the (PAA<sub>2</sub>)-Cu nanoparticles require the lowest activation energy (12.18 kJ mol<sup>-1</sup>) for reduction 2-NP and gave more favorable activation parameters  $\Delta H = 9.477$  kJ mol<sup>-1</sup> and  $\Delta S = -244.59$  J mol<sup>-1</sup> k<sup>-1</sup>. The constructed graphs shown in Fig. 12(a) represent the effect of different temperatures on the reduction ability of the prepared (PAA<sub>2</sub>)-Cu nanoparticles. Where it is noticed that, the time taken for reduction of 2-NP by using (PAA<sub>2</sub>)-Cu as a catalyst at 22°C, 36°C and 58°C was 160, 120 and 100 min, respectively.

#### 4. Conclusions

Different compositions of pectin-based hydrogels (PAA) were successfully prepared by gamma radiation and were examined for the in situ preparation of magnetic and metallic nanoparticles. The formation and size of nanoparticles were proved by XRD, SEM and TEM images of different nanocomposites. In addition, the PAA nanocomposites were examined for the reduction of 2-NP. PAA<sub>2</sub> nanocomposites loaded with different metals has the higher reduction ability for 2-NP than the other compositions. As the 2-NP concentration increased the reduction rate was decreased. The (PAA<sub>2</sub>)-Cu was required the lowest activation energy (12.18 kJ mol<sup>-1</sup>) for reduction 2-NP and (PAA/Fe<sub>3</sub>O<sub>4</sub>) loaded with Cu nanoparticles were shown superior reduction activity.

#### References

- [1] C.H. Liu, B.H. Chen, C.H. Hsueh, J.R. Ku, M.S. Jeng, F. Tsau, Hydrogen generation from hydrolysis of sodium borohydride using Ni-Ru nano-composite as catalysts, *J. Int. Hydrogen Energy*, 34 (2009) 2153–2163.
- [2] M. Zahmakiran, S. Ozkar, Zeolite framework stabilized rhodium (0) nano-clusters catalyst for the hydrolysis of ammonia-borane in air: outstanding catalytic activity, reusability and life time, *Appl. Catal., B*, 89 (2009) 104–110.
- [3] J.C. Ingersoll, N. Mani, J.C. Thenmozhiyal, A. Muthaiah, Catalytic hydrolysis of sodium borohydride by a novel nickel-cobalt-boride catalyst, *J. Power Sources*, 173 (2007) 450–457.
- [4] O. Metin, S. Ozkar, Hydrogen generation from the hydrolysis of sodium borohydride by using water dispersible, hydrogen phosphate-stabilized nickel nano-clusters as catalyst, *Int. J. Hydrogen Energy*, 32 (2007) 1707–1715.
- [5] H.B. Dai, Y. Liang, P. Wang, H.M. Cheng, Amorphous cobalt-boron/nickel foam as an effective catalyst for hydrogen generation from alkaline sodium borohydride solution, *J. Power Sources*, 177 (2008) 17–23.
- [6] D. Xu, P. Dai, X. Liu, C. Cao, Q. Guo, Carbon-supported cobalt catalyst for hydrogen generation from alkaline sodium borohydride solution, *J. Power Sources*, 182 (2008) 616–620.
- [7] J. Lee, K.Y. Kong, C.R. Jung, E. Cho, S.P. Yoon, J. Han, A structured Co-B catalyst for hydrogen extraction from NaBH<sub>4</sub> solution, *Catal. Today*, 120 (2007) 305–310.
- [8] J. Zhao, H. Ma, J. Chen, Improved hydrogen generation from alkaline NaBH<sub>4</sub> solution using carbon-supported Co-B as catalyst, *Int. J. Hydrogen Energy*, 32 (2007) 4711–4716.
- [9] K.S. Eom, K.W. Cho, H.S. Kwon, Effect of electron less deposition conditions on micro-structures of cobalt-phosphorous catalysts and their hydrogen generation properties in alkaline sodium borohydride solution, *J. Power Sources*, 180 (2008) 484–490.
- [10] D.R. Kim, K.W. Cho, Y.I. Choi, C.J. Park, Fabrication of porous Co-Ni-P catalysts by electro-deposition and their catalytic characteristics for the generation of hydrogen from an alkaline NaBH<sub>4</sub> solution, *Int. J. Hydrogen Energy*, 34 (2009) 2622–2630.
- [11] L. Qiu, Y. Peng, B. Liu, F. Yan, Polypyrrole nanotube-supported gold nanoparticles: an efficient electrocatalyst for oxygen reduction and catalytic reduction of 4-nitrophenol, *Appl. Catal., A*, 413–414 (2012) 230–237.
- [12] F. Liu, Y. Yuan, L. Li, S. Shang, X. Yu, Q. Zhang, S. Jiang, Y. Wu, Synthesis of polypyrrole nanocomposites decorated with silver nanoparticles with electrocatalysis and antibacterial property, *Composites Part B*, 69 (2015) 232–236.
- [13] L. Fangjun, Y. Yuan, L. Liang, S. Songmin, Y. Xianghua, Z. Qiao, J. Shouxiang, W. Yanguang, Synthesis of polypyrrole nanocomposites decorated with silver nanoparticles with electrocatalysis and antibacterial property, *Composites Part B*, 69 (2015) 232–236.
- [14] O. Akdim, U.B. Demirci, A. Brioude, P. Miel, Fluorinated cobalt for catalyzing hydrogen generation from sodium borohydride, *Int. J. Hydrogen Energy*, 34 (2009) 5417–5421.
- [15] G.A. Mahmoud, Adsorption of copper(II), lead(II), and cadmium(II) ions from aqueous solution by using hydrogel with magnetic properties, *Monatshefte für Chemie – Chemical Monthly*, 144 (2013) 1097–1106.
- [16] G.A. Mahmoud, Radiation synthesis of hydrogels as carriers for catalytic nanoparticles and their use in hydrogen production from sodium borohydride, *Monatshefte für Chemie – Chemical Monthly*, 145 (2014) 1–10.
- [17] L. Sibo, L. Jingya, Z. Xiaoya, L. Liang, Y. Xianghua, Assembly of conducting polypyrrole hydrogels as a suitable adsorbent for Cr (VI) removal, *Polym. Bull.*, 72 (2015) 2891–2902.
- [18] G.A. Mahmoud, S.E. Abdel-Aal, N.A. Badway, A.A. Elbayaa, D.F. Ahmed, A novel hydrogel based on agricultural waste for removal of hazardous dyes from aqueous solution and reuse process in a secondary adsorption, *Polym. Bull.*, 74 (2016). doi 10.1007/s00289-016-1717-0.

- [19] A. El-Hag Ali, A. Raafat, G.A. Mahmoud, N.A. Badway, M.A. El-Mottaleb, M.A. Elshahawy, Photocatalytic decolorization of dye effluent using radiation developed polymeric nanocomposites, *J. Inorg. Organomet. Polym. Mater.*, 26 (2016) 606–615.
- [20] S. Butun, N. Sahiner, Versatile hydrogel template for metal nano particle preparation and their use in catalysis, *Polymer*, 52 (2011) 4834–4840.
- [21] N. Sahiner, H. Ozaya, O. Ozaya, N. Aktas, New catalytic route: hydrogels as templates and reactors for in situ Ni nanoparticle synthesis and usage in the reduction of 2- and 4-nitrophenols, *Applied Catal.*, 385 (2010) 201–207.
- [22] N. Sahiner, S. Sagbas, The preparation of poly (vinyl phosphonic acid) hydrogels as new functional materials for in situ metal nanoparticle preparation, *Colloids Surf., A*, 418 (2013) 76–83.
- [23] T. Mingyi, Z. Sai, L. Xianxian, P. Xiaobo, Q. Haixia, Fabrication of magnetically recyclable Fe<sub>3</sub>O<sub>4</sub>@Cu nanocomposites with high catalytic performance for the reduction of organic dyes and 4-nitrophenol, *Mater. Chem. Phys.*, 148 (2014) 639–647.
- [24] A. Pamela, M. Sanjib, K. Jugal, G.S. Inderkumar, Synthesis of cobalt nano crystals in aqueous media and its characterization, *Mater. Sci. Appl.*, 2 (2011) 1307–1312.
- [25] Riyanto, R.O. Mohamed, Characterization of Ni-Co-PVC and Ni-Cu-PVC alloys prepared by mechanical alloying technique (MAT), *J. Open Mater. Sci.*, 2 (2008) 40–46.
- [26] A.M. Schmidt, Thermo-responsive magnetic colloids, *J. Colloid Polym. Sci.*, 258 (2007) 953–966.
- [27] Y. Nishio, A. Yamada, K. Ezaki, Y. Miyashita, H. Furukawa, K.J. Horie, Preparation and magnetometric characterization of iron oxide containing alginate/poly (vinyl alcohol networks), *Polymer*, 45 (2004) 7129–7140.
- [28] M. Nemanashi, R. Meijboom, Synthesis and characterization of Cu, Ag and Au dendrimer-encapsulated nanoparticles and their application in the reduction of 4-nitrophenol to 4-aminophenol, *J. Colloid Interface Sci.*, 389 (2013) 260–267.
- [29] P. Zhang, Y. Sui, G. Xiao, Y. Wang, C. Wang, B. Liu, G. Zou, B. Zou, Facile fabrication of faceted copper nanocrystals with high catalytic activity for p-nitrophenol reduction, *J. Mater. Chem. A*, 1 (2013) 1632–1638.
- [30] Z. Zhang, C. Shao, Y. Sun, J. Mu, M. Zhang, P. Zhang, Z. Guo, P. Liang, J. Wang, Y. Liu, Tubular nanocomposite catalysts based on sizecontrolled and highly dispersed silver nanoparticles assembled on electrospun silica nanotubes for catalytic reduction of 4-nitrophenol, *J. Mater. Chem.*, 22 (2012) 1387–1395.
- [31] J. Li, C.Y. Liu, Y. Liu, Au/graphene hydrogel: synthesis, characterization and its use for catalytic reduction of 4-nitrophenol, *J. Mater. Chem.*, 22 (2012) 8426–8430.